ACS Catalysis

Research Article

pubs.acs.org/acscatalysis

Mechanism of Aldehyde-Selective Wacker-Type Oxidation of Unbiased Alkenes with a Nitrite Co-Catalyst

Yuan-Ye Jiang,[†] Qi Zhang,[†] Hai-Zhu Yu,*[,‡] and Yao Fu*[,†]

[†]Collaborative Innovation Center of Chemistry for Energy Materials, CAS Key Laboratory of Urban Pollutant Conversion, Department of Chemistry, University of Science and Technology of China, Hefei 230026, China

[‡]Department of Polymer Science and Engineering, University of Science and Technology Beijing, 30 Xueyuan Road, Huasheng Building, Beijing 100083, China

Supporting Information

ABSTRACT: Traditional Wacker-type oxidations of unbiased alkenes produce ketones as major products. Recently, Grubbs' group reported a Wacker-type oxidation system in which aldehydes (rather than ketones) have been generated predominantly in the presence of a nitrite co-catalyst. To elucidate the mechanistic origin of the aldehyde selectivity, density functional theory (DFT) studies have been conducted in this study. Two oxymetalation pathways, i.e., *syn* addition and *anti* addition pathways, were considered for various possible active species including monomeric Pd, bimetallic Pd−Pd, heterobimetallic Pd−Cu, and heterobimetallic Pd−Ag complexes. It is found that *syn* addition is kinetically more favored than *anti* addition in general. Meanwhile, the most feasible oxymetalation processes occur on the heterobimetallic Pd−Cu complexes. Investigations on the subsequent aldehyde formation process show that 1,2-H shift mechanism on *t*BuOH-ligated Pd−Cu complexes is superior to the betaH-elimination mechanism. Besides, the 1,2-H shift is the rate- and regioselectivity-determining step of the whole catalytic cycle. The analysis on spin density population indicates that the *t*BuOH-ligated Pd−Cu complex promotes a radical 1,2-H shift on the oxygenated alkene. The longer Pd−C(alkene) distance facilitates the aldehyde-selective pathway (relative to the ketone-selective pathway) due to the stronger stability of the secondary carbon radical and the smaller distortion energy therein.

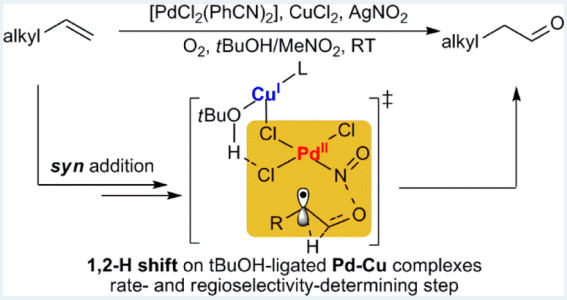

KEYWORDS: *Wacker oxidation, aldehyde, palladium, copper, radical, density functional theory, hydrogen transfer*

1. INTRODUCTION

The Wacker oxidation is a powerful tool for the catalytic synthesis of carbonyls from alkenes because of its high functional group tolerance and high efficiency.[1] Traditional Wacker-type oxidations produce ketones as the major products from terminal alkenes in accordance with Markovnikov's rule (Scheme 1A). With specific alkenes (such as aryl olefins or alkyl olefins linked with directing groups),[2,3] such regioselectivity has been successfully altered and aldehydes have been gained as the main products. The structural requirements of alkenes limited the utility of these reactions, and thus aldehyde-selective Wacker-type oxidations of unbiased alkenes has also been sought. Nevertheless, this issue remains challenging because the preliminary reports obtained only moderate aldehyde selectivity/yields.[4]

Recently, Grubbs et al. reported novel $[PdCl_2(PhCN)_2]$-$CuCl_2$-nitrite catalyzed Wacker-type oxidations in which aldehydes were gained predominantly from unbiased terminal alkenes (Scheme 1B).[5] The reactions occur smoothly at room temperature in the presence of the mixture of *t*BuOH and $MeNO_2$ (as solvent) and O_2 (as oxidant). Functional groups such as ether, nitro, carboxylic acid, ester, C_{sp2}-Br, and C_{sp3}-Br are well tolerated in this catalytic system. In addition, the highly selective generation of aldehydes was also achieved from protected allylic and homoallylic alcohols with this strategy.[6] To explore the mechanism of the interesting aldehyde selectivity, Grubbs et al. conducted a stoichiometric ^{18}O-labeling experiment and found that the carbonyl oxygen in the aldehyde products mainly comes from the nitrite salt. On this

Scheme 1. Traditional and Nitrite-Modified Wacker-Type Oxidations of Unbiased Alkenes Generate Different Regioselectivity

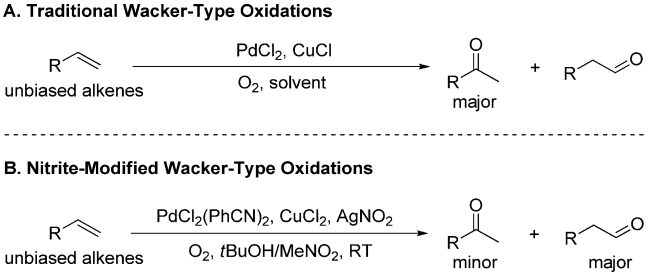

Received: November 26, 2014
Revised: January 14, 2015
Published: January 16, 2015

DOI: 10.1021/cs5018776
ACS Catal. 2015, 5, 1414−1423

basis, they proposed that metal mediated the delivery of NO_2 radical (generated in situ) to the alkene (Scheme 2A).

Scheme 2. Possible Active Catalysts for Nitrite-Modified Wacker Oxidations[a]

[a](a) Monomeric palladium complexes; (b) heterobimetallic Pd−Cu complexes; (c) heterobimetallic Pd−Ag complexes; (d) bimetallic Pd−Pd complexes.

Thereafter, NO is formed and aerobically oxidized into NO_2 to enable the catalytic use of the nitrite salts. What is more important is that the stoichiometric reaction of $CuCl_2$, $AgNO_2$, and alkene gave no conversion, implying that the NO_2 delivery may be accomplished by Pd.

Despite Grubbs' proposal on the active Pd catalysts and similar mechanistic discussions focusing on monomeric Pd catalysts,[7,8] some other possibilities still exist. In the early studies of Feringa et al. on the nitrite palladium and $CuCl_2$ catalyzed Wacker oxidation,[4a] a *t*BuOH-ligated heterobimetallic Pd−Cu catalyst is suggested to be determinant for the observed regioselectivity (Scheme 2B). Similarly, Hosokawa and Murahashi suggested the catalytic activity of the heterobimetallic Pd−Cu complex in their Wacker reactions without nitrites.[9] Sigman and Keith's kinetic studies also suggest that Cu salts are influential in Wacker oxidation of alkenes.[10] In addition, Goddard and co-workers' theoretical study indicates that the heterobimetallic Pd−Cu mechanism is slightly favored over the monomeric Pd mechanism in the Wacker reaction with H_2O as the oxygen source.[11] Meanwhile, the heterobimetallic Pd−Ag mechanism is also plausible in Grubbs' reactions because recently the Pd−Ag mechanism was found to be more plausible than the traditional monomeric-Pd mechanism in some other reactions (Scheme 2C). For example, very recently, Wu[12] and Schaefer[13] et al. found that a Pd−Ag complex-catalyzed pathway is more favored than the popular monomeric Pd pathway in some C−H functionalization reactions. Finally, the bimetallic Pd−Pd mechanism[14] in which $CuCl_2$ does not participate in the oxygen transfer step should also be considered (Scheme 2D).

Another important mechanistic question about the Wacker-type reaction is the detail of the oxymetalation step. Historically, the mechanism of oxymetalation for the traditional Wacker reactions has been longstanding and received wide attention[7] since its discovery in the late 1950s.[15] Henry originally proposed that two mechanisms might be responsible for the oxymetalation in Wacker oxidation, i.e., *syn* addition and *anti* addition (Scheme 3).[16] In *syn* addition, the oxygen source (H_2O or OH^-) and the catalyst locate at the same side of the

Scheme 3. Two Pathways of Oxymetallation in Wacker-Type Oxidations

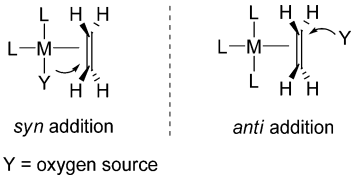

alkene and the oxygen source coordinates to the metal center. In *anti* addition, the oxygen source and the catalyst locates at the opposite side of alkenes, and no direct interaction exists between the metal center and the oxygen source. The experimental studies by Henry,[17] Akermark,[18] Kurosawa,[19] and Stille[20] et al. indicate that the dominant mechanism of oxymetalation for traditional Wacker reactions is *syn* addition at low [Cl^-] (<1.0 M) and [$CuCl_2$] (<1.0 M) concentrations and is *anti* addition at high [Cl^-] (>3.0 M) and [$CuCl_2$] (>2.5 M) concentrations.[11,21] Interestingly, the experimental and computational studies by Sigman and Keith in the absence of copper salts suggested an *anti* addition menchanism.[10] On the other hand, the mechanism of oxymetalation has also been extensively investigated by quantum-chemical and ab initio molecular dynamics methods.[7b] Those reports mostly supports *anti* addition[10,22] rather than *syn* addition.[11,23] In addition to the reports in which H_2O or OH^- act as the oxygen sources, the oxymetalation mechanism for *tert*-butylhydroperoxide-mediated Wacker-type reactions was recently investigated by Sigman et al. and *syn* addition was found to be favored.[24]

According to the aforementioned mechanistic understanding, many details on the nitrite-modified Wacker-type oxidations (such as the form of active catalysts, the pattern of oxymetalation, and especially the origin of the amazing aldehyde selectivity) has not been clarified. Theoretical study could provide preliminary mechanistic understanding and contribute to the further improvement of this type of reactions. For this purpose, a DFT study on the mechanism of the nitrite-modified Wacker-type reactions have been performed in the present study. Different from the traditional pathway of oxymetalation on monomeric palladium catalysts, the calculation results support *syn* addition on the heterobimetallic Pd−Cu complexes with a subsequent 1,2-H shift to generate aldehydes.

2. COMPUTATIONAL METHODS

All density functional theory calculations were conducted with the Gaussian 09 program.[25] Geometry optimization was performed with B3LYP method[26,27] in gas phase. 6-31G(d) basis set was used for main group elements and 6-311G(d) for Cu. LANL2DZ and the associated basis set[28] were used for Pd and Ag. Polarization functions were added for Pd (ζ(f) = 1.472) and Ag (ζ(f) = 1.611).[29] Frequency analysis was carried out at the same level of theory to verify the stationary points as an intermediate or transition state and to obtain the thermodynamic energy corrections. Intrinsic reaction coordinate (IRC) analysis[30] was conducted to check whether the transition states connect correct stationary points or not. Solution-phase single-point energy calculations were conducted on the basis of the gas-phase-optimized structures by using the B3LYP method and SMD solvation model (solvent = *t*BuOH). The 6-311+G(d,p) basis set was used for main group elements, 6-311G(d) for Cu and SDD basis set[31] for Pd and Ag. Dispersion corrections at the same level of theory were added by using the D3 version of Grimme's dispersion with Becke−Johnson damping to give a better description of long-range weak interactions.[32] A correction of 1.9 kcal/mol was added to account for the change from standard states in gas phase to aqueous solution.[11] The reported energies were the solution-phase single-point energies corrected by gas-phase thermodynamic energy corrections and solution-phase dispersion corrections. Both Gibbs free energies and enthalpies are presented and the following discussions are based on Gibbs

DOI: 10.1021/cs5018776
ACS Catal. 2015, 5, 1414−1423

free energies unless otherwise noted. The noncovalent interaction plot was generated with the NCIplot developed by Yang's group.[33]

3. RESULTS AND DISCUSSION

3.1. Model Reaction. The reaction of 1-butene and O_2 catalyzed by $[PdCl_2(PhCN)_2]$, $CuCl_2$, and $AgNO_2$ in *t*BuOH was used as the model reaction. Three major steps were considered for the investigated reaction (Scheme 4). First, the reactants generated the resting state of the catalysts by ligand exchange. Then oxymetalation occurred to form a C−O bond between NO_2 and the alkene. Finally, the formation of the major product (aldehyde) or the minor product (ketone) occurred and regenerated the catalyst to finish the whole catalytic cycle.

Scheme 4. Model Reaction and Considered Mechanism

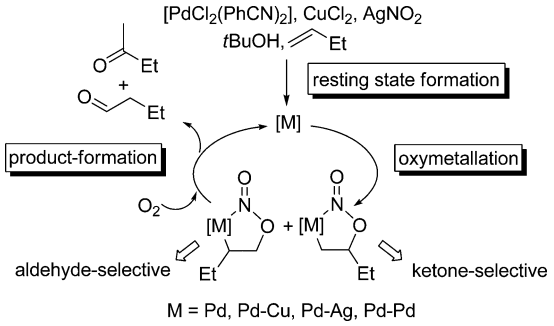

3.2. Resting State of Catalysts. The reactants could generate different monomeric Pd, bimetallic Pd−Cu, bimetallic Pd−Ag, and bimetallic Pd−Pd complexes.[34] The possible resting states of these catalysts were investigated. The most stable species for different types of catalysts are shown in Scheme 5, and the others are in the Supporting Information. It was found that three types of bimetallic Pd−Cu complexes,[35] i.e., bis(chloride)-bridged (**1** and **2**), mono(chloride)-bridged (**3**), and (chloride)(oxygen)-bridged complexes (**4**), are remarkably more stable than the other types of complexes. The free energies of **1**−**4** are −35.2, −35.2, −34.5, and −28.6 kcal/mol, respectively. Note that we also considered bis(oxygen)-bridged Pd−Cu complexes, but they are significantly less stable than **1**−**4** (Scheme S7 in Supporting Information). Meanwhile, **5**, **6**, and **7** are the most stable bimetallic Pd−Ag, monomeric Pd, and bimetallic Pd−Pd complexes, respectively. The free energies of **5**, **6**, and **7** are −19.3, −6.7, and −1.8 kcal/mol, respectively. In the next section, oxymetalation catalyzed by the different types of complexes was investigated.

3.3. Mechanism Study on Oxymetalation. Oxymetalation could proceed via either *syn* addition mechanism or *anti* addition mechanism as we mentioned in the Introduction. Herein, we investigated the possibility of *syn* addition mechanism first.

3.3.1. Oxymetalation through syn Addition Mechanism. In the following, we first examined the *syn* addition mechanism for the most stable catalysts **1** and **2**. As shown in Scheme 6, *syn* addition might occur from **1** via transition states **TS1a** and **TS1b**. **TS1a** is a ketone-selective transition state in which NO_2 attacks the substituted Csp^2 of the alkenes. **TS1b** is an aldehyde-selective transition state in which NO_2 attacks the nonsubstituted Csp^2 of the alkene. In **TS1a** and **TS1b**, the alkene coordinates to Pd and the NO_2 coordinates to Cu. From **1** to **TS1a**/**TS1b**, a distortion occurs to break the chloride bridging bond and make NO_2 close to the alkene. As shown in Figure 1, the Pd−Cu distance decreases from 2.960 Å in **1** to 2.473 Å in **TS1a** or 2.502 Å in **TS1b**. Similar to the *syn* addition on **1**, *syn* addition on **2** might also occur via two possible transition states **TS2a** and **TS2b**. Because NO_2 and the alkene both coordinate to Pd in **TS2a** and **TS2b**, they can approach each other without causing a significant structural distortion. As a result, **TS2a** and **TS2b** are almost planar (Figure 1). The free energies of **TS1a**, **TS1b**, **TS2a**, and **TS2b** are −8.5, −0.3,

Scheme 6. Calculated Free Energies (Enthalpies in Square Brackets) for Oxymetallation through *syn* Addition on Heterobimetallic Cu−Pd Complexes 1 and 2

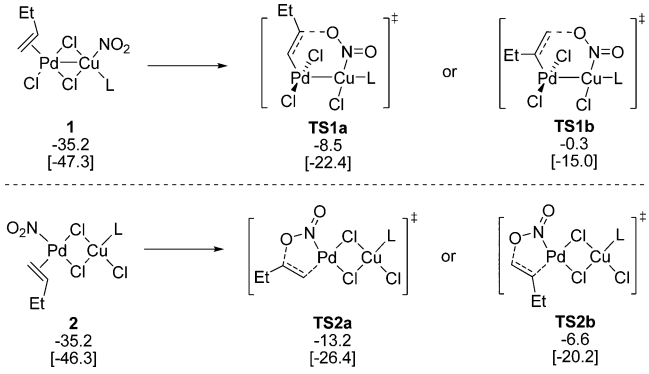

Scheme 5. Relative Free Energies of Structurally Representative Precatalysts (Enthalpies in Square Brackets)

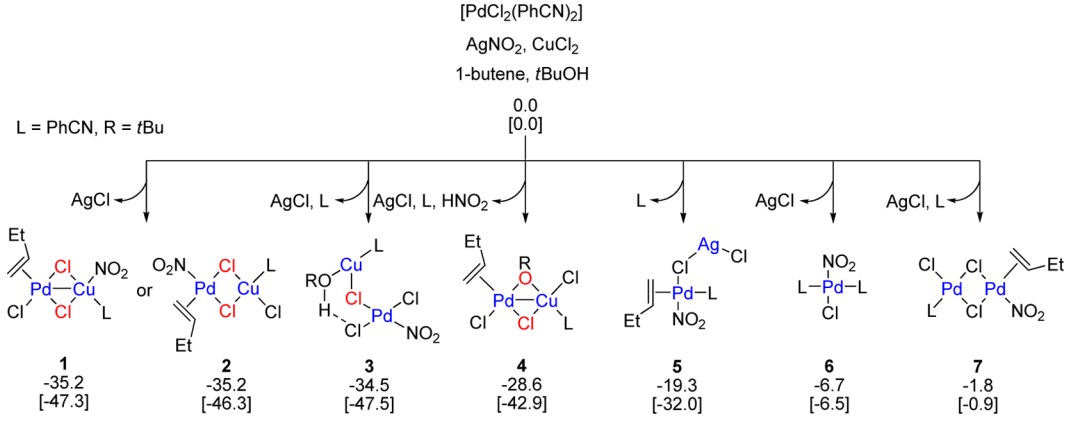

DOI: 10.1021/cs5018776
ACS Catal. 2015, 5, 1414−1423

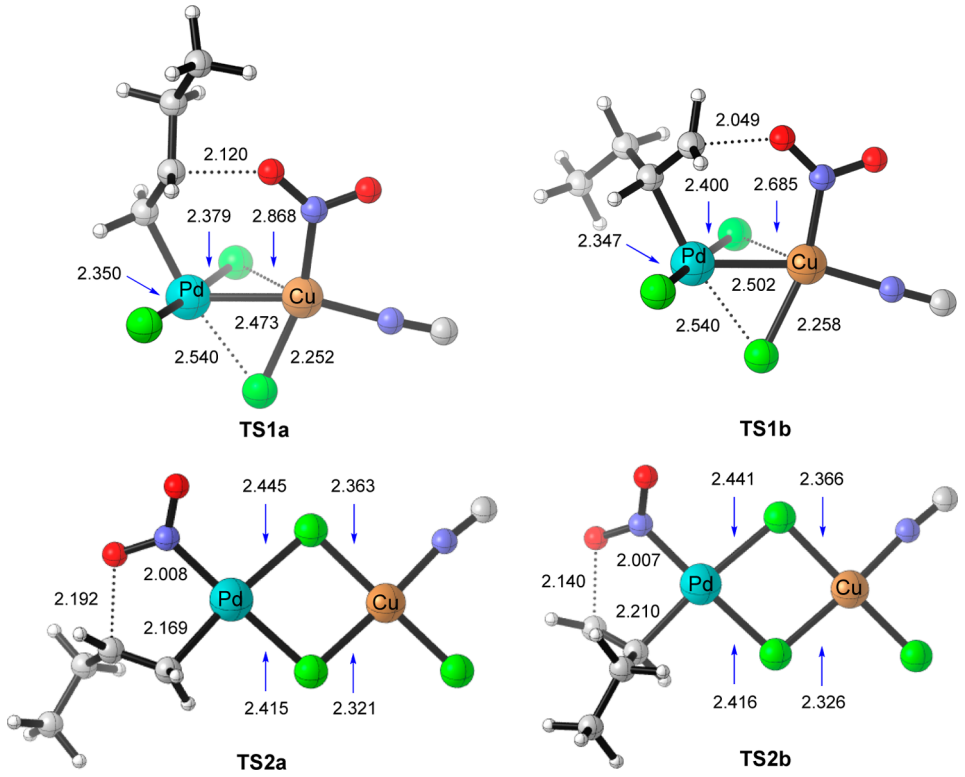

Figure 1. Optimized structures of *syn* and *anti* oxymetalation transition states on the heterobimetallic Pd−Cu complex **1** and **2** (bond length in Å). The phenyl group of PhCN was not shown for clarity reasons.

Scheme 7. Calculated Free Energies (Enthalpies in Square Brackets) for Oxymetallation through *syn* Addition on Heterobimetallic Pd−Cu Complexes 3 and 4[a]

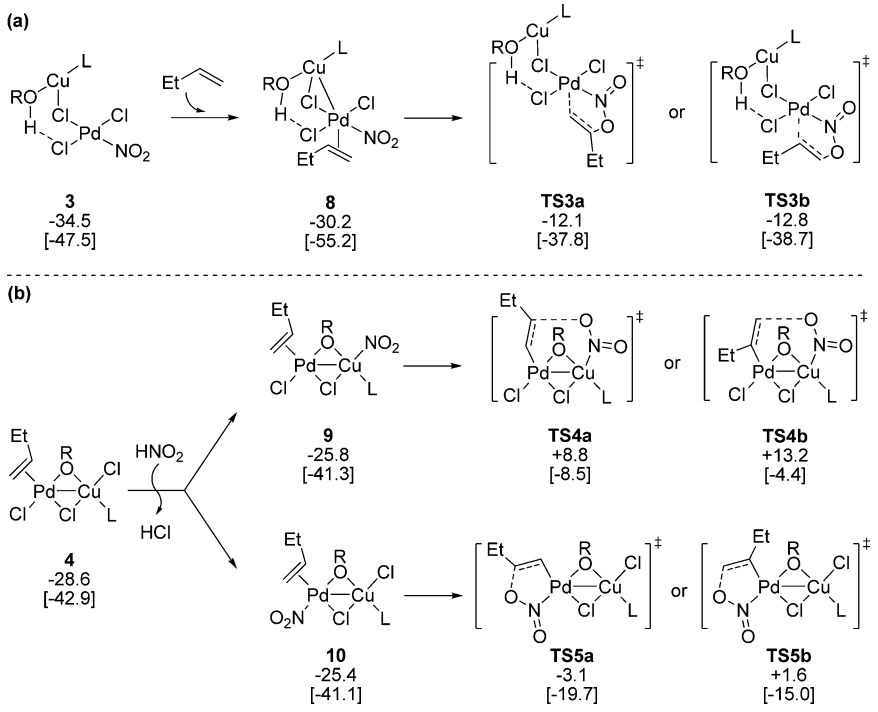

[a](a) *Syn* addition on heterobimetallic Pd−Cu complex **3**; (b) *syn* addition on heterobimetallic Pd−Cu complex **4**.

−13.2, and −6.6 kcal/mol, respectively. Thus, **TS2a** is the most stable one among them.

The mono(chloride)-bridged complex **3** generates **8** first by coordinating to the alkene, then oxymetalation occurs via the transition states **TS3a** and **TS3b** (Scheme 7a). **TS3a** is ketone selective and **TS3b** is aldehyde selective. The free energies of **TS3a** and **TS3b** are −12.1 and −12.8 kcal/mol respectively, and they are very close to the free energy of **TS2a** (−13.2 kcal/

DOI: 10.1021/cs5018776
ACS Catal. 2015, 5, 1414−1423

mol). This result indicates that **TS3a** and **TS3b** are competitive with **TS2a**.

Similarly, *syn* addition could occur on complex **4** (Scheme 7b). In this context, transformation of **4** to nitrite complexes **9** and **10** proceeds first.[36] Oxymetalation occurs from **9** via nonplanar transition states **TS4a** and **TS4b**, and it occurs from **10** via planar transition states **TS5a** and **TS5b**. Similar to the results in Scheme 6, **TS5a** is more stable than **TS4a**, **TS4b**, and **TS5b**. However, **TS5a** is less stable than **TS2a** by 10.1 kcal/mol, indicating that **TS5a** is less competitive.

The Pd−Ag complex **5** undergoes *syn* addition via **TS6a** and **TS6b** (Scheme 8). **TS6a** is more stable than **TS6b** by 7.3 kcal/mol, indicating that ketone selectivity is dominant for the *syn* addition on **5**. Finally, *syn* addition from monomeric Pd complex **6** and bimetallic Pd−Pd complex **7** was also considered. Ketone-selective oxymetalation was found to be favored but the free energy barriers were over 45 kcal/mol (refer to **1** or **2**), thus we excluded these two pathways (Scheme S8 in Supporting Information). According to the above results, **TS2a** is the most feasible *syn* addition transition state.

Scheme 8. Calculated Free Energies (Enthalpies in Square Brackets) for Oxymetallation through *syn* Addition on the Heterobimetallic Pd−Ag Complex 5

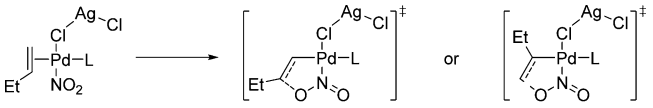

5 -19.3 [-32.0] **TS6a** +0.4 [-13.7] **TS6b** +7.7 [-6.6]

3.3.2. Oxymetalation through Anti Addition Mechanism. Similar to the discussions of the *syn* addition mechanism, the *anti* addition mechanism was also examined for complexes **1**−**7**. Among the investigated *anti*-addition transition states on different possible catalysts, **TS7a**, **TS7b**, **TS8a**, **TS8b**, **TS9a**, and **TS9b** were found to be relatively feasible (Scheme 9).

Scheme 9. Calculated Free Energies (Enthalpies in Square Brackets) for Oxymetallation through *anti* Addition from Heterobimetallic Pd−Cu Complexes 1−3

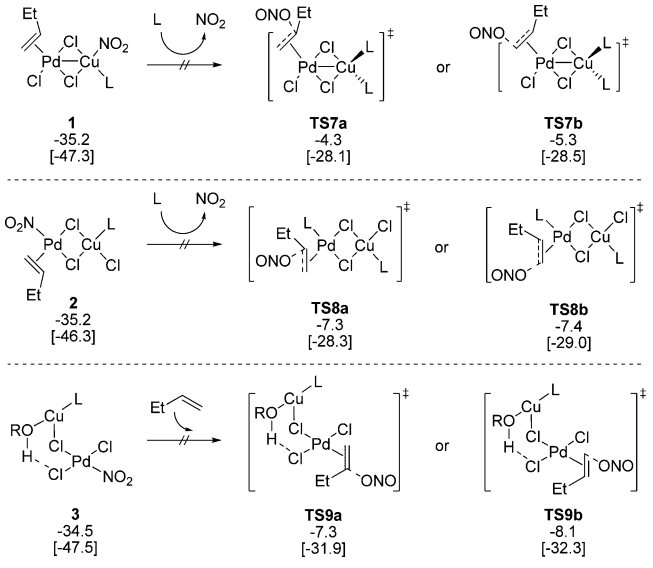

1 -35.2 [-47.3] **TS7a** -4.3 [-28.1] **TS7b** -5.3 [-28.5]

2 -35.2 [-46.3] **TS8a** -7.3 [-28.3] **TS8b** -7.4 [-29.0]

3 -34.5 [-47.5] **TS9a** -7.3 [-31.9] **TS9b** -8.1 [-32.3]

TS7a and **TS7b** are derived from the bimetallic Pd−Cu complex **1**, and their free energies are −4.3 and −5.3 kcal/mol, respectively. **TS8a** and **TS8b** are derived from **2** with free energies of −7.3 and −7.4 kcal/mol, respectively. The four transition states are all bis(chloride)-bridged. **TS9a** and **TS9b** are derived from **3**, and there is only one chloride bridging bond. The free energies of **TS9a** and **TS9b** are −7.3 and −8.1 kcal/mol. By contrast, the *anti* addition on all other species in Scheme 4, including the (chloride)(oxygen)-bridged complex **4**, Pd−Ag complex **5**, monomeric Pd complex **6**, and bimetallic Pd−Pd complex **7**, give remarkably higher free energy barrier (over 35 kcal/mol). For clarity reasons, the related results were put into the Supporting Information (Scheme S9). Taking these results into account, **TS9b** is the most feasible *anti* addition transition state. Nonetheless, **TS9b** is less stable than the most feasible *syn* addition transition state **TS2a** by 5.1 kcal/mol. Therefore, *syn* addition is kinetically more favorable than *anti* addition.

3.3.3. Regioselectivity of Oxymetalation. After investigating the oxymetalation transition states, we classified them into two groups, i.e., aldehyde-selective and ketone-selective, and arranged them in order of increasing free energy (Scheme 10). **TS3b** is the most feasible aldehyde-selective oxymetalation transition state with a free energy of −12.8 kcal/mol. **TS2a** is the most feasible ketone-selective oxymetalation transition state with a free energy of −13.2 kcal/mol. **TS2a** is more stable than **TS3b** by 0.4 kcal/mol, meaning that ketone selectivity is slightly dominant in the oxymetalation step. Therefore, the regioselectivity of oxymetalation could not explain the observed aldehyde selectivity in Grubbs experiments. Considering that the energy demands of several different oxymetalation steps are quite close and the regioselectivity is possibly determined by the subsequent steps, we performed calculations on the steps after oxymetalation. The products of several plausible oxymetalation processes (involving the aldehyde-selective transition states **TS3b**, **TS9b**, and **TS8b** and ketone-selective transition states **TS2a**, **TS3a**, and **TS1a**) were chosen for further investigations.[37]

Scheme 10. Calculated Free Energies (Enthalpies in Square Brackets) of Oxymetallation Transition States with Different Regioselectivity

aldehyde	**TS3b** -12.8 [-38.7]	**TS9b** -8.1 [-32.3]	**TS8b** -7.4 [-29.0]	**TS2b** -6.6 [-20.2]	**TS7b** -5.3 [-28.5]	**TS1b** -0.3 [-15.0]	**TS5b** +1.6 [-15.0] ···
ΔG_{sol}	⟶						
ketone	**TS2a** -13.2 [-26.4]	**TS3a** -12.1 [-37.8]	**TS1a** -8.5 [-22.4]	**TS9a** -7.3 [-31.9]	**TS8a** -7.3 [-28.3]	**TS7a** -4.3 [-28.1]	**TS5a** -3.1 [-19.7] ···

3.4. Mechanistic Study on Steps Following Oxymetalation. We started from the product of the most feasible aldehyde-selective oxymetalation transition state **TS3b** to investigate the following steps. As shown in Figure 2, **TS3b** derives from **3** by generating the active complex **8** first and affords the cyclopalladium complex **11**, causing an energy increase of 7.7 kcal/mol. From **11**, 1,2-H shift could occur via the transition state **TS10** with a free energy barrier of 14.7 kcal/mol. In **TS10**, the hydrogen atom on the terminal Csp^2 of the alkene transfers to the internal Csp^2 with a simultaneous N−O bond cleavage. The cracked N−O bond stretches from 1.394 Å in **11** to 1.925 Å in **TS10** (Figure 3). There is a chloride bridging bond in **TS10**, and the *t*BuOH on Cu also forms a

DOI: 10.1021/cs5018776
ACS Catal. 2015, 5, 1414−1423

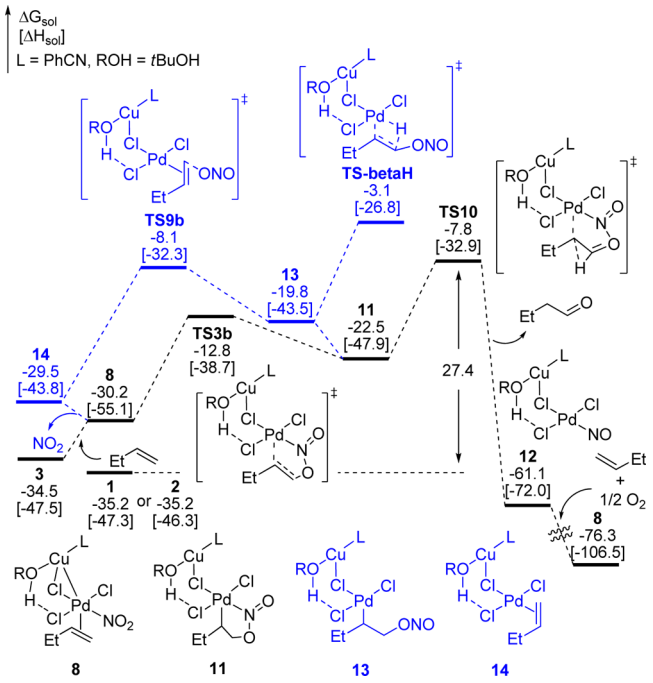

Figure 2. Calculated free energies (enthalpies in square brackets) for 1,2-H shift mechanism and betaH-elimination mechanism after oxymetalation on heterobimetallic Pd–Cu complexes.

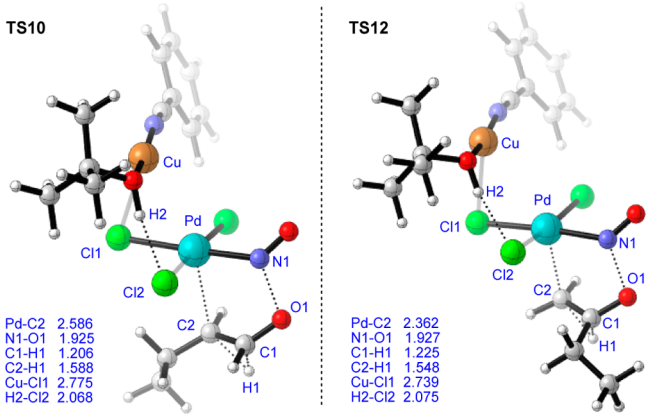

Figure 3. Optimized structures of 1,2-H shift transition state **TS10** and **TS12** (bond lengths in Å).

hydrogen bond with the chloride ligand on Pd (Figure S1 in Supporting Information). This process is akin to the proposed 1,2-hydride shift mechanism by Mimoun et al. in the Wacker oxidations with *tert*-butylhydroperoxide.[38] After **TS10**, the NO-coordinated complex **12** and the final product aldehyde are formed with a significant energy decrease of 53.3 kcal/mol, making the 1,2-H shift step irreversible. Finally, the aerobically oxidation of NO to NO_2 and the coordination of another alkene regenerate the active catalyst **8** with an energy decrease of 15.2 kcal/mol. According to Figure 2, **TS10** is the energetically highest point in this pathway.

We also considered the possibility of betaH-elimination for the product formation.[8a] This pathway was initiated by the isomerization of **11** to **13**. Then betaH-elimination occurred via transition state **TS-betaH**. However, **TS-betaH** is less stable than **TS10** by 4.7 kcal/mol, indicating that betaH-elimination is less competitive than 1,2-H shift, thus we excluded this pathway.

In addition to **TS3b**, **TS9b** could also occur from **8** by generating the intermediate **14** first (Figure 2). The transformation from **8** to **14** caused a slight energy increase of 0.7 kcal/mol. From **14**, **TS9b** affords the complex **13** and then isomerizes to **11** to undergo 1,2-H shift via **TS10**. Note that the relative free energy of **TS8b** and the other aldehyde-selective oxymetalation transition states (**TS2b**, **TS1b**...) is even higher than that of **TS10**, and therefore the pathways involving them are less competitive and we did not investigate their following processes. According to the above results, **8** → **TS3b** → **11** → **TS10** → **12** → **8** presents the most feasible catalytic cycle for aldehyde formation.

Next, we considered the following steps for the ketone-selective oxymetalation steps (Scheme 11). The most feasible

Scheme 11. Calculated Free Energies (Enthalpies in Square Brackets) for 1,2-H Shift Mechanism after the Feasible Ketone-Selective Oxymetallation Steps

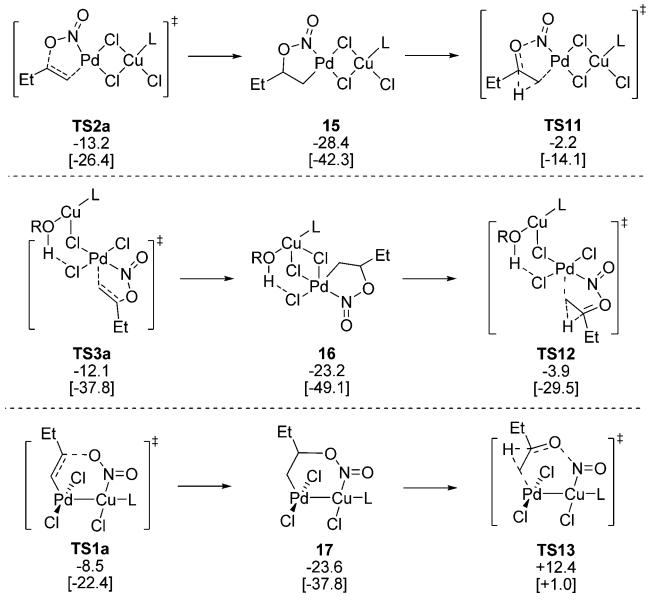

ketone-selective oxymetalation transition state **TS2a** generates the intermediate **15** with an energy decrease of 15.2 kcal/mol. Then 1,2-H shift occurs via bis(chloride)-bridged transition state **TS11**. Similarly, **TS3a** generates the intermediate **16** and affords the ketone product via 1,2-H shift transition state **TS12**. **TS1a** affords the ketone product through **17** and **TS12** successively. The free energies of **TS11**, **TS12**, and **TS13** are −2.2, −3.9, and +12.4 kcal/mol respectively, thus **TS12** is the most feasible one among them.

In **TS12**, there is a chloride bridging bond and a longer *t*BuOH-Cl bridging bond (Figure 3). **TS12** is structurally akin to **TS10** but less stable than **TS10** by 3.9 kcal/mol. Besides, the other ketone-selective oxymetalation transition states are also less stable than **TS10**, thus aldehyde-selective pathways are more feasible and this is consistent with the experimental observations.

It should be pointed that we also examined the possibilities of high-spin states (triplet and quartet) of heterobimetallic Pd–Cu complexes, monomeric Pd complexes, bimetallic Pd–Pd complexes, and heterobimetallic Pd–Ag complexes. However, the free energies of all the high spin states are higher than the related low-spin one by at least 10 kcal/mol (Table S2 in Supporting Information). For example, the free energies of the

DOI: 10.1021/cs5018776
ACS Catal. 2015, 5, 1414–1423

related quartet states of **TS10**, **11**, and **8** are +16.9, +6.8, and −16.3 kcal/mol respectively, much higher than those of the doublet states (−7.8, −22.5, and −30.2 kcal/mol, respectively). According to these results, the concerned reaction tends to proceed on low-spin heterobimetallic Pd−Cu complexes.

3.5. Overall Mechanism. Taking all the results above into account, we could get the overall mechanism of the nitrite-modified Wacker-type oxidation of unbiased alkenes. As shown in Figure 4, the catalytic cycle starts with forming the active

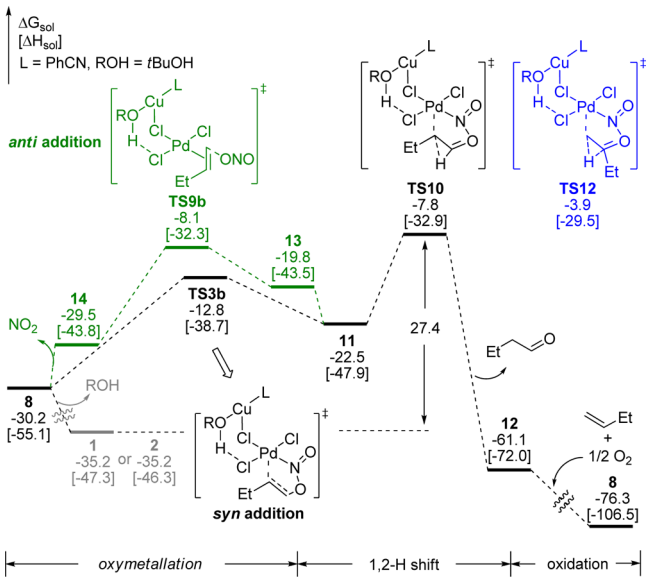

Figure 4. Calculated energy profile of the nitrite-modified Wacker-type oxidation of unbiased alkenes.

heterobimetallic nitrite Pd−Cu complex **8** from the precursors. The rapid oxymetalation of alkene on **8** then occurred via *syn* addition transition state **TS3b** and generated the transient cyclometal complex **11**. Note that *anti* addition mechanism (**8** → **14** → **TS9b** → **13** → **11**) could also generate **11** but is kinetically less favorable than *syn* addition mechanism (via **TS3b**). From intermediate **11**, 1,2-H shift occurs via **TS10**, affording the aldehyde product and the NO-coordinated complex **12**. This process (**8** → **TS3b** → **11** → **TS10**) is relatively more favorable than the ketone-selective 1,2-H shift step (via **TS12**). The formation of the aldehyde product is highly exergonic and irreversible. Finally, the oxidation of NO into NO_2 and the coordination of another alkene regenerate **8** to finish the whole catalytic cycle.

According to the energetic span model developed by Kozuch and Shaik,[39] the energy barrier of a catalytic cycle is related to the energy span between the turnover-determining intermediate (TDI) and turnover-determining transition state (TDTS). **1** and **2** are the most stable forms of catalysts, and **TS10** is the highest energetic point in the energy profile. In the concept of energetic span model, **1** (or **2**) is the TDI and **TS10** is the TDTS. The overall energy barrier of the catalytic cycle should be the energy difference between **TS10** and **1** (or **2**), i.e., +27.4 kcal/mol. This result seems to be high for the Grubbs' reactions occurring in room temperature. Analyzing the reason for such observation, we suggest that the overestimated free energy barrier originated from the overestimated entropy effect. The entropy effect I ignorable when the numbers of reactants and products are equal, whereas it become significant when the numbers are not equal.[40,41] To settle this problem, we corrected the entropy effect with Sakaki's method, which omits the entropy contributions of translation and rotation movements[41] and found that **8** is more stable than **1** and **2** by 3.3 and 4.7 kcal/mol, respectively.[42] In this situation, **8** is the TDI and the overall energy barrier is the energy span of **8** and **TS10**, i.e., +22.4 kcal/mol, consistent with the Grubbs' experimental conditions. Note that Sakaki's strategy does not affect our main conclusion that *syn* addition on *t*BuOH-ligated heterobimetallic Pd−Cu complexes with subsequent 1,2-H shift is the most feasible mechanism for the concerned reaction. Therefore, Gibbs free energy is used for discussions in sections 3.2, 3.3, and 3.4 for the sake of convenience.

3.6. Origin of Aldehyde Selectivity. The above calculation results show that 1,2-H shift is the regioselectivity-determining step. Among the investigated 1,2-H shift transition state, **TS10** is the most feasible aldehyde-selective one and **TS12** is the most feasible ketone-selective one. Both **TS10** and **TS12** are heterobimetallic Pd−Cu species with similar structures. The most remarkable structural difference between **TS10** and **TS12** lies in the Pd−C2 bond lengths (Figure 3). The Pd−C2 distance is 2.586 Å in **TS10** and 2.362 Å in **TS12** with a difference of 0.224 Å. The larger Pd−C2 distance in **TS10** might result in the lower repulsion between the organic moiety and the metal catalyst. Accordingly, we propose that the structures of heterobimetallic Pd−Cu complexes play an important role.

To verify the above proposal, we divided **TS10**/**TS12** into two parts, i.e., the organic moiety constituting products **TSX-org** and the rest **TSX-metal** (X = 10 or 12), and calculated the electronic energies of the two parts (Scheme 12).[43] **TS10-org** and **TS10-metal** are more stable than **TS12-org** and **TS12-metal** by 0.8 and 1.1 kcal/mol, respectively, supporting that the structural distortions are smaller in **TS10**.

Scheme 12. Calculated Electronic Energies of the Fragments of Key 1,2-H Shift Transition States (kcal/mol)

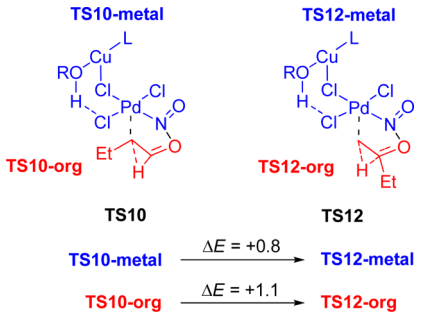

We finally made efforts in analyzing the origin of the relatively longer catalyst−substrate distance in **TS10**. From the spin density plot in Figure 5, it can be seen that the spin density of the radical mainly spreads around the Pd, NO_2, and alkene in **TS10** and **TS12**, implying that spin transfers from the radical organic species ($EtC\dot{H}CH_2O$ in **TS10** and $EtCH(O)\dot{C}H_2$ in **TS12**) to the NO-coordinated metal species. Because the primary carbon radical is less stable than secondary carbon radical, a shorter Pd−C2 distance is needed in **TS12** to stabilize the primary carbon radical ($EtCH(O)\dot{C}H_2$) with the interaction with the metal center. By contrast, a weaker Pd−C2 interaction is adequate to stabilize the secondary carbon radical ($Et\dot{C}HCH_2O$), thus a longer Pd−C2 distance is allowed

DOI: 10.1021/cs5018776
ACS Catal. 2015, 5, 1414−1423

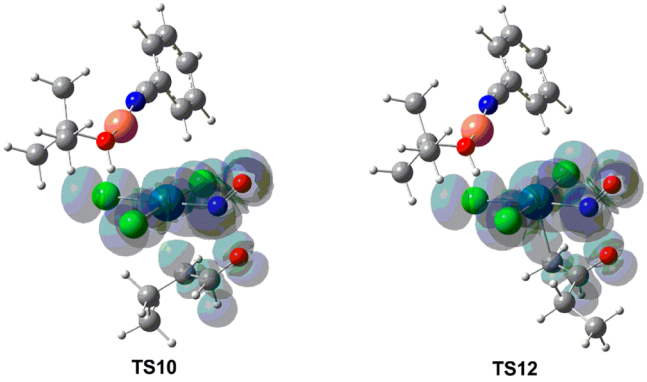

Figure 5. Spin density population of key 1,2-H shift transition states (isovalue = 0.0004).

in **TS10**. This result induces a smaller distortion energy in **TS10** and contributes to the observed aldehyde-selectivity.

4. CONCLUSIONS

Nitrite-modified Wacker-type oxidation of unbiased alkenes represents a novel strategy for the synthesis of aldehydes and expands the utilities of Wacker oxidations. To explore the origin of the aldehyde selectivity, a mechanistic study was conducted with the aid of density functional theory methods. The following conclusions have been gained:

1. The most feasible mechanism involves the in situ generation of *t*BuOH-ligated heterobimetallic nitrite Pd−Cu complexes. The subsequent oxymetalation occurs via *syn* addition mechanism to afford a cyclometal intermediate. Then 1,2-H shift from the cyclometallic intermediate directly affords the aldehyde product and a NO-coordinated Pd−Cu complex. Aerobically oxidation of NO to NO_2 finally regenerates the active Pd−Cu species to finish the catalytic cycle. 1,2-H shift is the rate- and regioselectivity-determining step of the whole catalytic cycle.

2. *syn* addition is kinetically more favorable than *anti* addition in the oxymetalation step, and both of them are reversible in the whole catalytic cycle.

3. Both palladium and copper catalysts participate in the favorable mechanism by forming the heterobimetallic Pd−Cu complexes. The solvent *t*BuOH also contributes to the stabilities of the Pd−Cu complexes by forming a hydrogen bond with the chloride ligand.

4. The origin of the aldehyde selectivity lies in that the *t*BuOH-ligated nitrite Pd−Cu complex promotes a radical 1,2-H shift on the oxygenated alkene. A longer distance between the metal catalyst and the alkene is allowed in the aldehyde-selective case due to the stronger stability of secondary carbon radical therein. This phenomenon lowers the steric hindrance, leads to smaller distortion energies, and contributes to the aldehyde selectivity finally.

As the first theoretical study on the mechanism of aldehyde-selective Wacker-type oxidation of unbiased alkenes, the present study proposed a novel heterobimetallic Pd−Cu complexes mediated radical pathway. This mechanism is different from the polar pathways on monomeric Pd complexes in traditional Wacker-type oxidations. Because of the complexity of the concerned Wacker reaction system, more detailed experimental and theoretical mechanistic studies are currently underway to verify the proposed mechanism.

■ ASSOCIATED CONTENT

Supporting Information

The following file is available free of charge on the ACS Publications website at DOI: 10.1021/cs5018776

Details of possible resting states of precatalysts and less feasible oxymetalation processes; energies and Cartesian coordinates of all calculated intermediates and transition states (PDF)

■ AUTHOR INFORMATION

Corresponding Authors

*E-mail: yuhz@ustb.edu.cn.

*E-mail: fuyao@ustc.edu.cn.

Notes

The authors declare no competing financial interest.

■ ACKNOWLEDGMENTS

We thank the NSFC (21325208, 21172209, 21361140372, 21202006), the 973 Program (2012CB215306), FRFCU (WK2060190025, WK2060190040, FRF-TP-14-015A2), CAS (KJCX2-EW-J02), PCSIRT, and the supercomputer center of Shanghai and USTC.

■ REFERENCES

(1) (a) Tsuji, J. *Synthesis* **1984**, 369−384. (b) Punniyamurthy, T.; Velusamy, S.; Iqbal, J. *Chem. Rev.* **2005**, *105*, 2329−2363. (c) Cornell, C. N.; Sigman, M. S. *Inorg. Chem.* **2007**, *46*, 1903−1909. (d) Kotov, V.; Scarborough, C. C.; Stahl, S. S. *Inorg. Chem.* **2007**, *46*, 1910−1923. (e) Tsuji, J. *Palladium Reagents and Catalysts: New Perspectives for the 21st Century*; John Wiley & Sons, Ltd: New York, 2004; pp 27−103. (f) Jira, R. *Angew. Chem., Int. Ed.* **2009**, *48*, 9034−9037. (g) McDonald, R. I.; Liu, G.; Stahl, S. S. *Chem. Rev.* **2011**, *111*, 2981−3019. (h) Sigman, M. S.; Werner, E. W. *Acc. Chem. Res.* **2012**, *45*, 874−884. (i) Shi, Z.; Zhang, C.; Tang, C.; Jiao, N. *Chem. Soc. Rev.* **2012**, *41*, 3381−3430.

(2) For selected examples see: (a) Dong, J. J.; Fananas-Mastral, M.; Alsters, P. L.; Browne, W. R.; Feringa, B. L. *Angew. Chem., Int. Ed.* **2013**, *52*, 5561−5565. (b) Teo, P.; Wickens, Z. K.; Dong, G.; Grubbs, R. H. *Org. Lett.* **2012**, *14*, 3237−3239. (c) Yamamoto, M.; Nakaoka, S.; Ura, Y.; Kataoka, Y. *Chem. Commun.* **2012**, *48*, 1165−1167. (d) Dong, G.; Teo, P.; Wickens, Z. K.; Grubbs, R. H. *Science* **2011**, *333*, 1609−1612. (e) Weiner, B.; Baeza, A.; Jerphagnon, T.; Feringa, B. L. *J. Am. Chem. Soc.* **2009**, *131*, 9473−9474.

(3) For more examples, please see: Muzart, J. *Tetrahedron* **2007**, *63*, 7505−7521.

(4) (a) Feringa, B. L. *J. Chem. Soc., Chem. Commun.* **1986**, 909−910. (b) Wenzel, T. T. *J. Chem. Soc., Chem. Commun.* **1993**, 862−864. (c) Ogura, T.; Kamimura, R.; Shiga, A.; Hosokawa, T. *Bull. Chem. Soc. Jpn.* **2005**, *78*, 1555−1557.

(5) (a) Wickens, Z. K.; Morandi, B.; Grubbs, R. H. *Angew. Chem., Int. Ed.* **2013**, *52*, 11257−11260. (b) Bronner, S. M.; Grubbs, R. H. *Chem. Sci.* **2014**, *5*, 101−106.

(6) Wickens, Z. K.; Skakuj, K.; Morandi, B.; Grubbs, R. H. *J. Am. Chem. Soc.* **2014**, *136*, 890−893.

(7) For reviews on Wacker reactions: (a) Keith, J. A.; Henry, P. M. *Angew. Chem., Int. Ed.* **2009**, *48*, 9038−9049. (b) Stirling, A.; Nair, N. N.; Lledós, A.; Ujaque, G. *Chem. Soc. Rev.* **2014**, *43*, 4940−4952.

(8) For some selected examples: (a) Ye, X.; Liu, G.; Popp, B. V.; Stahl, S. S. *J. Org. Chem.* **2011**, *76*, 1031−1044. (b) Keith, J. A.; Oxgaard, J.; Goddard, W. A. *J. Am. Chem. Soc.* **2006**, *128*, 3132−3133. (c) McDonald, R. I.; White, P. B.; Weinstein, A. B.; Tam, C. P.; Stahl, S. S. *Org. Lett.* **2013**, *13*, 2830−2833. (d) Cornell, C. N.; Sigman, M. S. *J. Am. Chem. Soc.* **2005**, *127*, 2796−2797.

(9) (a) Hosokawa, T.; Nomura, T.; Murahashi, S.-I. *J. Organomet. Chem.* **1998**, *551*, 387−389. (b) Hosokawa, T.; Aoki, S.; Takano, M.;

DOI: 10.1021/cs5018776
ACS Catal. 2015, 5, 1414−1423

Nakahira, T.; Yoshida, Y.; Murahashi, S.-I. *J. Chem. Soc., Chem. Commun.* **1991**, 1559−1560.
(10) Anderson, B. J.; Keith, J. A.; Sigman, M. S. *J. Am. Chem. Soc.* **2010**, *132*, 11872−11874.
(11) Keith, J. A.; Nielsen, R. J.; Oxgaard, J.; Goddard, W. A. *J. Am. Chem. Soc.* **2007**, *129*, 12342−12343.
(12) Yang, Y.-F.; Cheng, G.-J.; Liu, P.; Leow, D.; Sun, T.-Y.; Chen, P.; Zhang, X.; Yu, J.-Q.; Wu, Y.-D.; Houk, K. N. *J. Am. Chem. Soc.* **2014**, *136*, 344−355.
(13) Anand, M.; Sunoj, R. B.; Schaefer, H. F. *J. Am. Chem. Soc.* **2014**, *136*, 5535−5538.
(14) Bimetallic Pd−Pd complexes are also suggested to be the active catalysts in some Pd-catalyzed reactions, see: (a) Powers, D. C.; Ritter, T. *Nature Chem.* **2009**, *1*, 302−309. (b) Bonney, K. J.; Proutiereab, F.; Schoenebeck, F. *Chem. Sci.* **2013**, *4*, 4434−4439. (c) Chan, W.-W.; Zhou, Z.; Yu, W.-Y. *Chem. Commun.* **2013**, *49*, 8214−8216.
(15) Smidt, J.; Hafner, W.; Jira, R.; Sedlmeier, J.; Sieber, R.; Rüttinger, R.; Kojer, H. *Angew. Chem.* **1959**, *71*, 176−182.
(16) Henry, P. M. *J. Am. Chem. Soc.* **1964**, *86*, 3246−3250.
(17) (a) Francis, J. W.; Henry, P. M. *J. Mol. Catal. A: Chem.* **1995**, *99*, 77−86. (b) Wan, W. K.; Zaw, K.; Henry, P. M. *Organometallics* **1988**, *7*, 1677−1683. (c) Francis, J. W.; Henry, P. M. *Organometallics* **1991**, *10*, 3498−3503. (d) Francis, J. W.; Henry, P. M. *Organometallics* **1992**, *11*, 2832−2836. (e) Henry, P. M.; Hamed, O.; Thompson, C. *J. Org. Chem.* **1997**, *62*, 7082−7083. (f) Hamed, O.; Henry, P. M.; Thompson, C. *J. Org. Chem.* **1999**, *64*, 7745−7750.
(18) (a) Akermark, B.; Söderberg, B. C.; Hall, S. S. *Organometallics* **1987**, *6*, 2608−2610. (b) Bäckvall, J.-E.; Akermark, B.; Ljunggren, S. O. *J. Chem. Soc., Chem. Commun.* **1977**, 264−265. (c) Bäckvall, J.-E.; Akermark, B.; Ljunggren, S. O. *J. Am. Chem. Soc.* **1979**, *101*, 2411−2416.
(19) Majima, T.; Kurosawa, H. *J. Chem. Soc., Chem. Commun.* **1977**, 610−611.
(20) Stille, J. K.; Divakaruni, R. *J. Am. Chem. Soc.* **1978**, *100*, 1303−1304.
(21) (a) Keith, J. A.; Nielsen, R. J.; Oxgaard, J.; Goddard, W. A. *Organometallics* **2009**, *28*, 1618−1619.
(22) (a) Bäckvall, J.-E.; Bjorkman, E. E.; Pettersson, L.; Siegbahn, P. *J. Am. Chem. Soc.* **1984**, *106*, 4369−4373. (b) Fujimoto, H.; Yamasaki, T. *J. Am. Chem. Soc.* **1986**, *108*, 578−581. (c) Siegbahn, P. E. M. *J. Phys. Chem.* **1996**, *100*, 14672−14680. (d) Kragten, D.; van Santen, R. A.; Lerou, J. J. *J. Phys. Chem. A* **1999**, *103*, 80−88. (e) Beyramabadi, S. A.; Eshtiagh-Hosseini, H.; Housaindokht, M. R.; Morsali, A. *Organometallics* **2008**, *27*, 72−79. (f) Comas-Vives, A.; Stirling, A.; Lledós, A.; Ujaque, G. *Chem.—Eur. J.* **2010**, *16*, 8738−8747. (g) Nair, N. N. *J. Phys. Chem. B* **2011**, *115*, 2312−2321. (h) Kovács, G.; Stirling, A.; Lledós, A.; Ujaque, G. *Chem.—Eur. J.* **2012**, *18*, 5612−5619. (i) Imandi, V.; Kunnikuruvan, S.; Nair, N. N. *Chem.—Eur. J.* **2013**, *19*, 4724−4731.
(23) Nelson, D. J.; Li, R.; Brammer, C. *J. Am. Chem. Soc.* **2001**, *123*, 1564−1568.
(24) Michel, B. W.; Steffens, L. D.; Sigman, M. S. *J. Am. Chem. Soc.* **2011**, *133*, 8317−8325.
(25) Frisch, M. J.; Trucks, G. W.; Schlegel, H. B.; Scuseria, G. E.; Robb, M. A.; Cheeseman, J. R.; Scalmani, G.; Barone, V.; Mennucci, B.; Petersson, G. A.; Nakatsuji, H.; Caricato, M.; Li, X.; Hratchian, H. P.; Izmaylov, A. F.; Bloino, J.; Zheng, G.; Sonnenberg, J. L.; Hada, M.; Ehara, M.; Toyota, K.; Fukuda, R.; Hasegawa, J.; Ishida, M.; Nakajima, T.; Honda, Y.; Kitao, O.; Nakai, H.; Vreven, T.; Montgomery, J. A. Jr.; Peralta, J. E.; Ogliaro, F.; Bearpark, M.; Heyd, J. J.; Brothers, E.; Kudin, K. N.; Staroverov, V. N.; Keith, T.; Kobayashi, R.; Normand, J.; Raghavachari, K.; Rendell, A.; Burant, J. C.; Iyengar, S. S.; Tomasi, J.; Cossi, M.; Rega, N.; Millam, J. M.; Klene, M.; Knox, J. E.; Cross, J. B.; Bakken, V.; Adamo, C.; Jaramillo, J.; Gomperts, R.; Stratmann, R. E.; Yazyev, O.; Austin, A. J.; Cammi, R.; Pomelli, C.; Ochterski, J. W.; Martin, R. L.; Morokuma, K.; Zakrzewski, V. G.; Voth, G. A.; Salvador, P.; Dannenberg, J. J.; Dapprich, S.; Daniels, A. D.; Farkas, O.; Foresman, J. B.; Ortiz, J. V.; Cioslowski, J.; Fox, D. J.; *Gaussian 09*, revision D.01; Gaussian, Inc.: Wallingford CT, 2013.
(26) (a) Becke, A. D. *J. Chem. Phys.* **1993**, *98*, 5648−5652. (b) Lee, C.; Yang, W.; Parr, R. G. *Phys. Rev. B* **1988**, *37*, 785−789.
(27) B3LYP method is widely used for mechanistic studies on Pd- and Cu-catalyzed reactions: (a) Zhang, S. L.; Liu, L.; Fu, Y.; Guo, Q. X. *Organometallics* **2007**, *26*, 4546−4554. (b) Nova, A.; Suh, H.-W.; Schmeier, T. J.; Guard, L. M.; Eisenstein, O. *Angew. Chem., Int. Ed.* **2014**, *53*, 1103−1108. (c) Cheng, G.-J.; Yang, Y.-F.; Liu, P.; Chen, P.; Sun, T.-Y.; Li, G.; Zhang, X.; Houk, K. N.; Yu, J.-Q.; Wu, Y.-D. *J. Am. Chem. Soc.* **2014**, *136*, 894−897. (d) Zhang, S. L.; Fu, Y.; Shang, R.; Guo, Q. X.; Liu, L. *J. Am. Chem. Soc.* **2010**, *132*, 638−646. (e) Yang, Y.-F.; Cheng, G.-J.; Liu, P.; Leow, D.; Sun, T.-Y.; Chen, P.; Zhang, X.; Yu, J.-Q.; Wu, Y.-D.; Houk, K. N. *J. Am. Chem. Soc.* **2014**, *136*, 344−355. (f) Yu, H.-Z.; Jiang, Y.-Y.; Fu, Y.; Liu, L. *J. Am. Chem. Soc.* **2010**, *132*, 18078−18091. (g) Tsai, M.-L.; Hadt, R. G.; Vanelderen, P.; Sels, B. F.; Schoonheydt, R. A.; Solomon, E. I. *J. Am. Chem. Soc.* **2014**, *136*, 3522−3529.
(28) (a) Hay, P. J.; Wadt, W. R. *J. Chem. Phys.* **1985**, *82*, 270−283. (b) Hay, P. J.; Wadt, W. R. *J. Chem. Phys.* **1985**, *82*, 299−310.
(29) Ehlers, A. W.; Bohme, M.; Dapprich, S.; Gobbi, A.; Hollwarth, A.; Jonas, V.; Kohler, K. F.; Stegmann, R.; Veldkamp, A.; Frenking, G. *Chem. Phys. Lett.* **1993**, *208*, 111−114.
(30) (a) Fukui, K. *J. Phys. Chem.* **1970**, *74*, 4161−4163. (b) Fukui, K. *Acc. Chem. Res.* **1981**, *14*, 363−368.
(31) Andrae, D.; Haussermann, U.; Dolg, M.; Stoll, H.; Preuss, H. *Theor. Chim. Acta* **1990**, *77*, 123−141.
(32) (a) Grimme, S. *J. Comput. Chem.* **2006**, *27*, 1787−1799. (b) Grimme, S.; Antony, J.; Ehrlich, S.; Krieg, H. *J. Chem. Phys.* **2010**, *132*, 154104. (c) Grimme, S.; Ehrlich, S.; Goerigk, L. *J. Comput. Chem.* **2011**, *32*, 1456−1465.
(33) Johnson, E. R.; Keinan, S.; Mori-Sánchez, P.; Contreras-García, J.; Cohen, A. J.; Yang, W. *J. Am. Chem. Soc.* **2010**, *132*, 6498−6506.
(34) Note that the spices NO_2 appears in the manuscript indicates NO_2 radical or NO_2^- if not mentioned because the two forms are both possible and depend on the distribution of spin density of NO_2-containing species.
(35) For the crystal structures of heterobimetallic Pd−Cu complexes see: (a) Hosokawa, T.; Takano, M.; Murahashi, S.-I. *J. Am. Chem. Soc.* **1996**, *118*, 3990−3991. (b) Hosokawa, T.; Takano, M.; Murahashi, S.-I.; Ozaki, H.; Kitagawa, Y.; Sakaguchi, K.-i.; Katsube, Y. *J. Chem. Soc., Chem. Commun.* **1994**, 1433−1434. (c) Dutta, B.; Adhikary, B.; Flörke, U.; Nag, K. *Eur. J. Inorg. Chem.* **2006**, 4111−4122. (d) Panther, T.; Behrens, U. *Z. Anorg. Allg. Chem.* **2000**, *626*, 1934−1941.
(36) **8**, **9**, and **10** could also be directly formed from the precursor catalysts $[PdCl_2(PhCN)_2]$, $CuCl_2$, and $AgNO_2$ (Scheme S5, S6).
(37) If subsequent pathways of the chosen oxymetalation products are found to be energetically higher than the rest oxymetalation transition states, we will continue to investigate the subsequent pathways for the rest oxymetalation transition states as well.
(38) (a) Mimoun, H.; Charpentier, R.; Mitschler, A.; Fischer, J.; Weiss, R. *J. Am. Chem. Soc.* **1980**, *102*, 1047−1054. (b) Roussel, M.; Mimoun, H. *J. Org. Chem.* **1980**, *45*, 5387−5390.
(39) (a) Kozuch, S.; Shaik, S. *Acc. Chem. Res.* **2011**, *44*, 101−110. (b) Kozuch, S.; Shaik, S. *J. Phys. Chem. A* **2008**, *112*, 6032−6041.
(40) Several correction methods are currently available to settle the overestimated entropy effect: (a) Dieckmann, A.; Houk, K. N. *Chem. Sci.* **2013**, *4*, 3591−3600. (b) Ribeiro, R. F.; Marenich, A. V.; Cramer, C. J.; Truhlar, D. G. *J. Phys. Chem. B* **2011**, *115*, 14556−14562. (c) Huang, F.; Lu, G.; Zhao, L.; Li, H.; Wang, Z.-X. *J. Am. Chem. Soc.* **2010**, *132*, 12388−12396. (d) Xie, H.; Lin, Z. *Organometallics* **2014**, *33*, 892−897. (e) Wertz, D. H. *J. Am. Chem. Soc.* **1980**, *102*, 5316−5322. (f) Leung, B. O.; Reid, D. L.; Armstrong, D. A.; Rauk, A. *J. Phys. Chem. A* **2004**, *108*, 2720−2725. (g) Ardura, D.; López, R.; Sordo, T. L. *J. Phys. Chem. B* **2005**, *109*, 23618−23623. (h) Chen, P.; Dougan, B. A.; Zhang, X.; Wu, Y.-D.; Xue, Z.-L. *Polyhedron* **2013**, *58*, 30−38.
(41) Sugiyama, A.; Ohnishi, Y.-y.; Nakaoka, M.; Nakao, Y.; Sato, H.; Sakaki, S.; Nakao, Y.; Hiyama, T. *J. Am. Chem. Soc.* **2008**, *130*, 12975−12985.

DOI: 10.1021/cs5018776
ACS Catal. 2015, 5, 1414−1423

(42) Currently, we are not able to exclude the possibility that the overestimated barrier is originated from the tunneling effect of hydrogen transfer.
(43) Similar structural decomposition strategy have been reported: (a) Yang, Z.; Yu, H.; Fu, Y. *Chem.—Eur. J.* **2013**, *19*, 12093−12103. (b) Lill, S. O. N.; Ryberg, P.; Rein, T.; Bennstr, E.; Norrby, P.-O. *Chem.—Eur. J.* **2012**, *18*, 1640−1649. (c) Ess, D. H.; Houk, K. N. *J. Am. Chem. Soc.* **2007**, *129*, 10646−10647.

DOI: 10.1021/cs5018776
ACS Catal. 2015, 5, 1414−1423